Semifluorinated Aromatic Side-Group Polystyrene-Based Block Copolymers: Bulk Structure and Surface Orientation Studies

Xuefa Li,[†] Luisa Andruzzi,[†,‡] Emo Chiellini,[‡] Giancarlo Galli,[‡] Christopher K. Ober,*[,†] Alexander Hexemer,[§] Edward J. Kramer,[§,||] and Daniel A. Fischer[⊥]

Department of Materials Science and Engineering, Cornell University, Ithaca, New York 14853, Dipartimento di Chimica e Chimica Industriale, Università di Pisa, 56126 Pisa, Italy, Department of Materials, University of California, Santa Barbara, California 93106, Department of Chemical Engineering, University of California, Santa Barbara, California 93106, and Materials Science & Engineering Laboratory, National Institute of Standards and Technology, Gaithersburg, Maryland 20899

Received March 22, 2002

ABSTRACT: Two families of narrow polydispersity poly(styrene)-based block copolymers bearing side groups containing both a phenyl ring and a *para*-linked semifluorinated side group were designed to produce stable low energy surfaces. The effects of the phenyl ring on the surface and bulk structure of the materials were investigated. The semifluorinated side chains were found to self-assemble into liquid-crystalline smectic layers within the microphase domains. An unexpected enhancement of surface organization by the aromatic group was observed. The bulk morphology and the interplay between microphase separation and liquid crystalline self-assembly were examined using transmission electron microscopy and X-ray scattering. Near-edge X-ray absorption fine structure (NEXAFS) studies were used to probe the surface coverage of the fluorinated segments. NEXAFS also allowed the determination of the orientation parameters (S_{C-F} and S_{π^*}) of the C−F bond and phenyl ring of the semifluorinated side groups at the surface. On the basis of these data, the orientational coupling between the $-CF_2-$ helix and the aromatic ring was found to depend on the length of the fluorocarbon substituent.

Introduction

Fluorinated polymers represent a class of very interesting and versatile polymeric materials which may find application in many different fields[1] ranging from electronics[2] and optics[3] to coatings,[4] thanks to their outstanding properties such as low dielectric constant,[5] low refractive index and high transparency,[6−8] as well as chemical and thermal resistance.[9]

The incorporation of fluorine in a polymer causes the polymer to have a low surface energy[10,11] potentially leading to low wettability, low friction coefficient and low adhesion.[12−16] Long term hydrophobicity even after exposure to a polar fluid, such as water, may arise in particular when the fluorinated side chains of a polymer are capable of organizing into an ordered structure both in the bulk and at the surface in such a way that leads to the formation of a surface primarily composed of tightly packed $-CF_3$ groups.[1,17,18] These unique characteristics render fluorinated polymers particularly suitable for applications such as hydrophobic, nonadherent coatings. Our previous investigations, focusing on block copolymers bearing semifluorinated alkyl side chains, showed that the self-assembly behavior of the semifluorinated side groups led to well organized low energy surfaces. Those surfaces were quite stable to reconstruction upon exposure to water when there were eight $-(CF_2)-$ units and between four and ten $-(CH_2)-$ units in the semifluorinated side chain.[1,17,18]

Furthermore, fluorinated block copolymers present the additional advantage that they can segregate to the surface of a polymer coating, driven there by the low surface energy of the fluorinated block.[19] As a consequence, they may find application as surface modifiers since a small amount of the fluorinated block copolymer can be blended with the corresponding nonfluorinated homopolymer to impart low surface energy behavior to the blend. This approach is particularly interesting for technological applications because it permits the production of low surface energy coatings using a minimum amount of fluorinated polymeric material. The goal of the present research was to develop new block copolymers bearing fluorinated substituents containing aromatic groups in the side chains, capable in principle of improving the properties of the surface by exploiting the enhanced self-assembly behavior of the semifluorinated side groups containing a phenyl ring.

Bearing this idea in mind we synthesized two series of new fluorinated block copolymers by following two different synthetic paths, on the one hand using the polymer-analogous modification reaction of the side chains of preformed anionically polymerized poly(styrene-*b*-isoprene) block copolymers and on the other the controlled radical polymerization of fluorinated styrene monomers.

The synthesis and the liquid-crystalline behavior of the polymers are reported elsewhere.[20] In the present study the bulk morphology of the synthesized semifluorinated block copolymers was characterized by transmission electron microscopy and X-ray diffraction, and their surface organization was evaluated by near-edge X-ray absorption fine structure (NEXAFS). The effects of the phenyl ring on the orientation of the fluorinated substituent at the surface was elucidated by relating the surface order parameter of the $-CF_2-$ helix, S_{C-F}, with the surface order parameter of the phenyl ring normal, S_{π^*}. Finally, the structure of the fluorinated

[†] Department of Materials Science and Engineering.
[‡] Dipartimento di Chimica e Chimica Industriale.
[§] Department of Materials.
[||] Department of Chemical Engineering.
[⊥] Materials Science & Engineering Laboratory.

10.1021/ma020463k CCC: $22.00
Published on Web 09/14/2002

Scheme 1. Chemical Structures of Side Chain Modified Block Copolymers via Anionic Polymerization

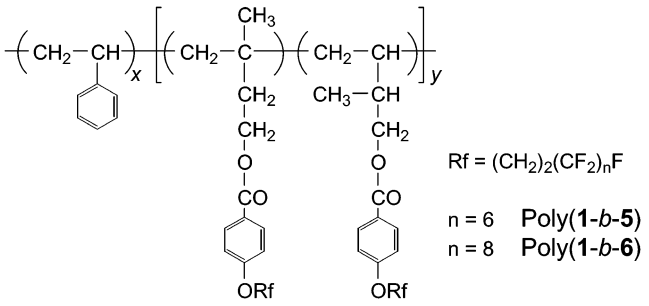

Scheme 2. Chemical Structures of Block Copolymers via Controlled Radical Polymerization

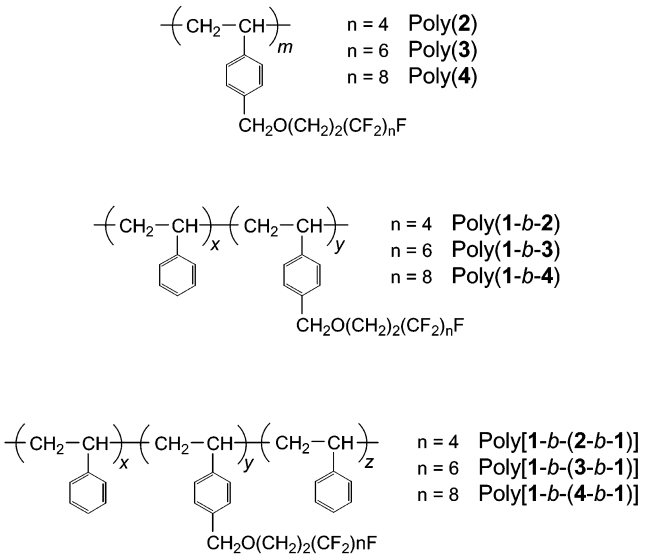

Table 1. Characterization Data of Block Copolymers from Polymer-Analogous Modification.

sample	M_n[a] (kg/mol)	M_w/M_n[a]	% side chain modification[b]	compn$_{FB}$[c] (wt %)
poly(**1**-*b*-**5**)	64	1.12	96	64
poly(**1**-*b*-**6**)	63	1.13	94	69

[a] Determined by GPC in THF. [b] Determined by ^{1}H NMR. [c] Weight % of the fluorinated block (FB) determined by ^{1}H NMR.

surface as revealed by NEXAFS was correlated to the wetting behavior of the materials.

Experimental Section

Materials. The two series of block copolymers were synthesized by polymer-analogous modification reaction of preformed anionic block copolymers and by controlled radical polymerization, respectively. The corresponding chemical structures are shown in Schemes 1 and 2, respectively. Both synthetic routes led to narrow polydispersity block copolymers characterized by different block length ratios (See Table 1 and Table 2). A detailed description of the synthesis is given in ref 20.

Characterization of Block Copolymers. Small-angle X-ray scattering (SAXS) studies were performed at the Cornell High Energy Synchrotron Source (CHESS) using monochromatic X-rays with a wavelength $\lambda = 0.155$ nm and a charge coupled detector (CCD). The X-ray intensity and the distance between the sample and the CCD detector could be easily adjusted according to the needs of the experiment. Films of thickness ≈0.5 mm cast from 5 wt % trifluorotoluene solutions were analyzed. The solvent was allowed to evaporate slowly

Table 2. Characterization Data of Block Polymers via Controlled Radical Polymerization.

sample	M_n[a] (kg/mol)	M_w/M_n[a]	compn$_{FB}$[b] (wt %)
poly(**2**)[c]	21	2.5	100
poly(**3**)[c]	15	2.5	100
poly(**4**)[c]	n.d.[d]	n.d.	100
poly(**1**-*b*-**2**)	18	1.3	88
poly(**1**-*b*-**3**)	18	1.3	87
poly(**1**-*b*-**4**)	n.d.	n.d.	92
poly[**1**-*b*-(**2**-*b*-**1**)]	110	1.4	50
poly[**1**-*b*-(**3**-*b*-**1**)]	65	1.4	49

[a] Determined by GPC in chloroform. [b] Weight % of the fluorinated block (FB) determined by ^{1}H NMR. [c] Reference fluorinated homopolymers prepared by conventional free radical polymerization. [d] n.d. = not determined.

for 1 week at room temperature. Then the as-cast films were dried thoroughly under vacuum at room temperature for 2 days to remove residual solvent and annealed at 145 °C under vacuum for 4 days to improve long-range order of the morphology. The annealing temperature of 145 °C was far enough (≈40 °C) above the glass transition of the PS block to allow mobility of the chains.

For TEM studies, small pieces of the above polymer films were embedded in epoxy resin which was cured at 70 °C for 6 h to produce samples suitable for cross-sectional ultramicrotomy. Thin sections (approximately 60 nm thick) were microtomed at room temperature and stained with RuO_4 vapors for 15−20 min. The RuO_4 preferentially stains PS microdomains leading to an enhanced electron scattering contrast between the fluorinated and the PS blocks. A JEOL 1200EX transmission electron microscope operated at 120 kV was used to image these thin sections.

The NEXAFS experiments were carried out on the NIST/Dow materials characterization end station on the U7A beamline at the National Synchrotron Light Source at Brookhaven National Laboratory. The beam line is equipped with a toroidal mirror spherical grating monochromator that gives this beamline an incident photon energy resolution and intensity of 0.2 eV and 5×10^{10} photons/s, respectively, for an incident photon energy of 300 eV and a typical storage ring current of 500 mA. The X-rays are elliptically polarized, with the electric field vector dominantly in the plane of the storage ring (polarization factor = 0.85).

The end-station is equipped with a heating/cooling stage positioned on a goniometer that controls the orientation of the sample with respect to the polarization vector of the X-rays. A differentially pumped ultrahigh vacuum compatible proportional counter is used for collecting the fluorescence yield (FY) signal. In addition, the partial-electron-yield (PEY) is collected using a channeltron electron multiplier with an adjustable entrance grid bias. All the data reported here are for an entrance grid bias (EGB) of −150V. To eliminate the effect of incident beam intensity fluctuations and monochromator absorption features, the FY and PEY signals were normalized by the incident beam intensity obtained from the photo yield of a clean gold grid.

Polymer films approximately 200 nm thick were prepared by spin-coating 5% trifluorotoluene polymer solutions onto silicon wafers. These films were then annealed for 6 h at 150 °C under vacuum. Contact angles were measured using a NRL contact angle goniometer model 100−00 (Ramé-Hart Inc.) at room temperature. The contact angles were averaged over four measurements. Polymer films were prepared by spin-coating 5 wt % trifluorotoluene polymer solutions on a silica wafer followed by annealing for 15 h in a vacuum oven at 150 °C. Linear alkanes (heptane, octane, nonane, undecane, dodecane, and tetradecane) were used as standards to measure the critical surface tension.

Results and Discussion

It is our goal to report the bulk and surface structure characterization of two series of new poly(styrene)-based

Table 3. Thermal Characterization Data of Polymers Studied in This Paper

sample	LC mesophase transition temperature (°C)[a]
poly(**2**)	G 14 S_I[b] 127 I[c]
poly(**3**)	G 17 S_I 133 I
poly(**4**)	G 50 S_I 67 S_{II} 190 I
poly(**1**-*b*-**2**)	G_I 17 G_{II} 69 S_I 137 I
poly(**1**-*b*-**3**)	G_I 17 S_I 152 I
poly(**1**-*b*-**4**)	G_I 52 S_I 68 S_{II} 180 I
poly[**1**-*b*-(**2**-*b*-**1**)]	G 106 S_I 125 I
poly[**1**-*b*-(**3**-*b*-**1**)]	G 106 S_{II} 154 I
poly[**1**-*b*-(**4**-*b*-**1**)]	G 106 S_I 185 I
poly(**1**-*b*-**5**)	G_I −32 G_{II} 101 S_I 207 I
poly(**1**-*b*-**6**)	G_I −20 G_{II} 100 S_I 210 I
F8H10	S_B 49.9 S_A 72.2 I

[a] Determined by temperature-dependent WAXD. [b] Details of smectic mesophase (S_I and S_{II}) are being studied. [c] G indicates glass state while I indicates isotropic state.

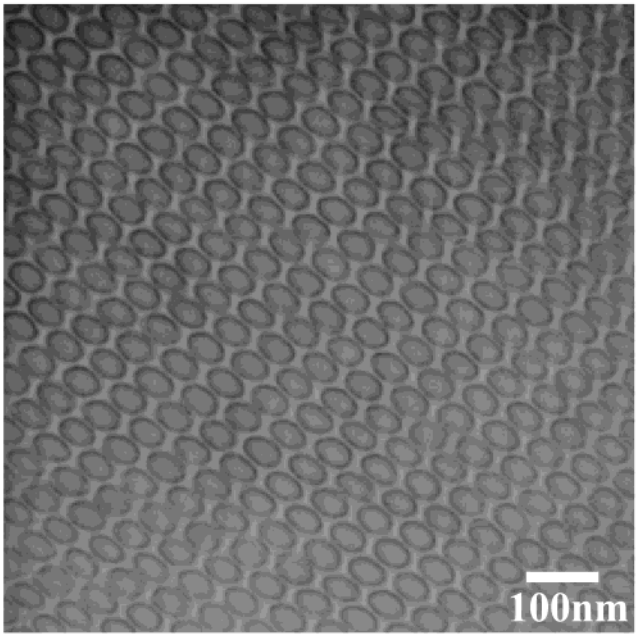

Figure 1. TEM micrograph of sample poly(**1**-***b***-**5**) with 64 wt % of semifluorinated block. Polystyrene block was stained by RuO_4 and appears dark.

block copolymers bearing fluoroalkyl-substituted aromatic side chains (see Schemes 1 and 2), while studying the effects of the phenyl ring on the surface structure and properties of the materials. As reported elsewhere,[20] all the fluorinated polymers formed a layered smectic mesophase at room temperature and increasing the length of the side-chain fluorocarbon tail enhanced the degree of order of the mesophase. In particular, in passing from $(CF_2)_4$ to $(CF_2)_8$, the nature of the detected mesophase changed from a disordered smectic to a hexatic smectic. The GPC and ^1H NMR characterization data of the block copolymers are reported in Tables 1 and 2, while the thermal characterization data are reported in Table 3.

Morphology Studies. The block copolymer morphologies were studied by small-angle X-ray scattering (SAXS) and transmission electron microscopy (TEM). The observed microstructures were consistent with our previous studies of block copolymers with LC side groups. TEM revealed that block copolymers with PS wt fraction ∼30−35% have cylindrical microstructures consisting of polystyrene cylinders in a fluorinated

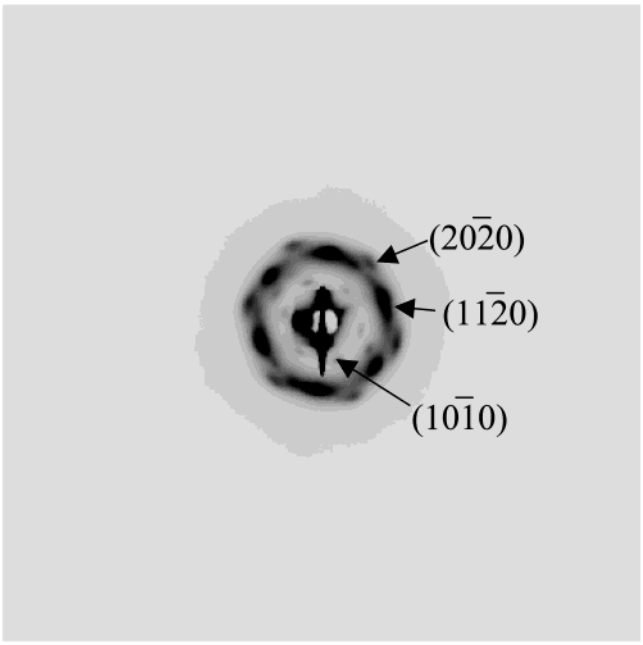

Figure 2. Two-dimensional SAXS pattern of sample poly(**1**-***b***-**5**) showing a hexagonal structure corresponding to the TEM micrograph in Figure 1.

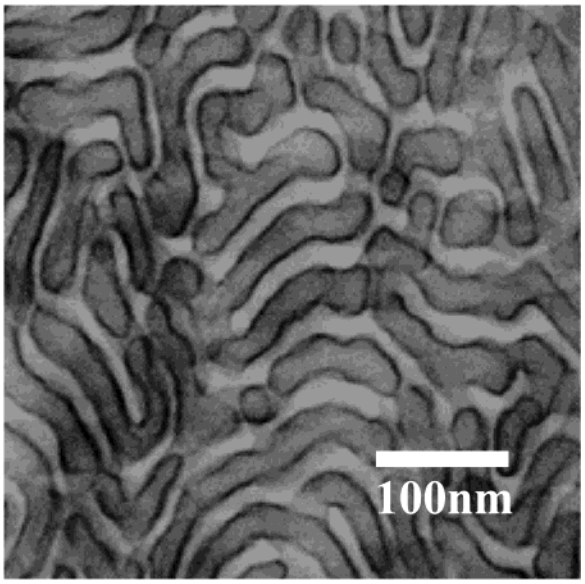

Figure 3. TEM micrograph of sample poly(**1**-***b***-**6**) with 69 wt % of semifluorinated block. Polystyrene block was stained by RuO_4 and appears dark.

liquid-crystalline matrix, as expected from the weight compositions reported in Table 1. In particular, poly(**1**-***b***-**5**) was found to self-organize into a highly ordered hexagonally packed cylindrical morphology as illustrated in the TEM images in Figure 1.

SAXS studies carried out on a poly(**1**-***b***-**5**) sample, carefully aligned so that the axes of the cylinders were parallel to the X-ray beam, confirmed the hexagonal cylinder nature of the morphology as can be seen from the SAXS pattern shown in Figure 2. An analysis of the above pattern showed that the inner 6 diffraction spots correspond to diffraction index {10−10} with a domain spacing of 52 nm, which was in good agreement with the domain spacing calculated from TEM images. This sample interestingly can form highly ordered large single-domain hexagonal cylinders by simple film cast-

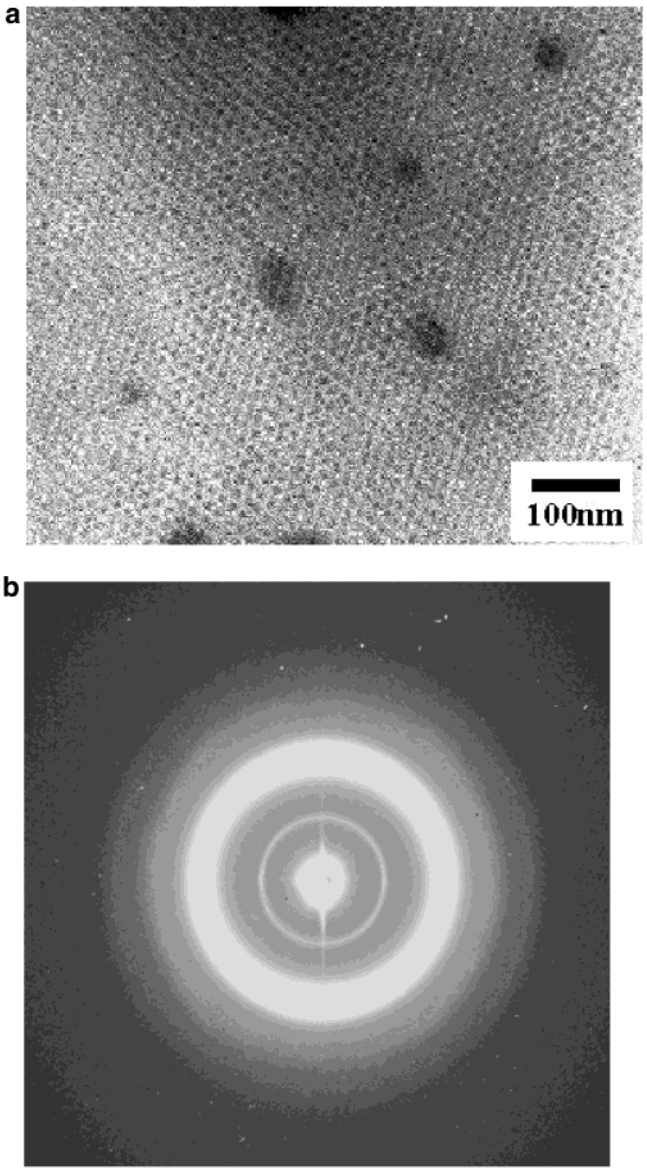

Figure 4. (a) TEM micrograph of sample poly(**1-*b*-4**). This polystyrene block with 8 wt % composition forms a body centered cubic ordered phase of spheres and was preferentially stained by RuO_4. (b) Two-dimensional SAXS patterns of sample poly(**1-*b*-4**). The inner weak ring in the SAXS pattern was attributed to diffraction from the second harmonic of the synchrotron X-ray beam.

ing. In contrast to poly(**1-*b*-5**), poly(**1-*b*-6**) showed a microphase-separated wormlike cylinder morphology lacking in orientation. The cylinder domain size determined from TEM was ∼40 nm as shown in Figure 3.

Diblock copolymers, with FB content ∼90 wt % were found to have a spherical morphology with poly(styrene) spheres placed in a LC matrix, as expected from the copolymer compositions reported in Table 2. The spherical domain sizes obtained from TEM were 15 nm, 15 nm and 17 nm for poly(**1-*b*-2**), poly(**1-*b*-3**), and poly(**1-*b*-4**), respectively. The spherical morphology was confirmed by SAXS to be typical for the body centered cubic phase morphology. These three samples showed very similar SAXS patterns and TEM micrographs. As an example, a typical SAXS pattern and a TEM image for sample poly(**1-*b*-4**) are shown in Figure 4. The weak inner ring in the SAXS pattern was attributed to diffraction from the second harmonic of the synchrotron X-ray beam.

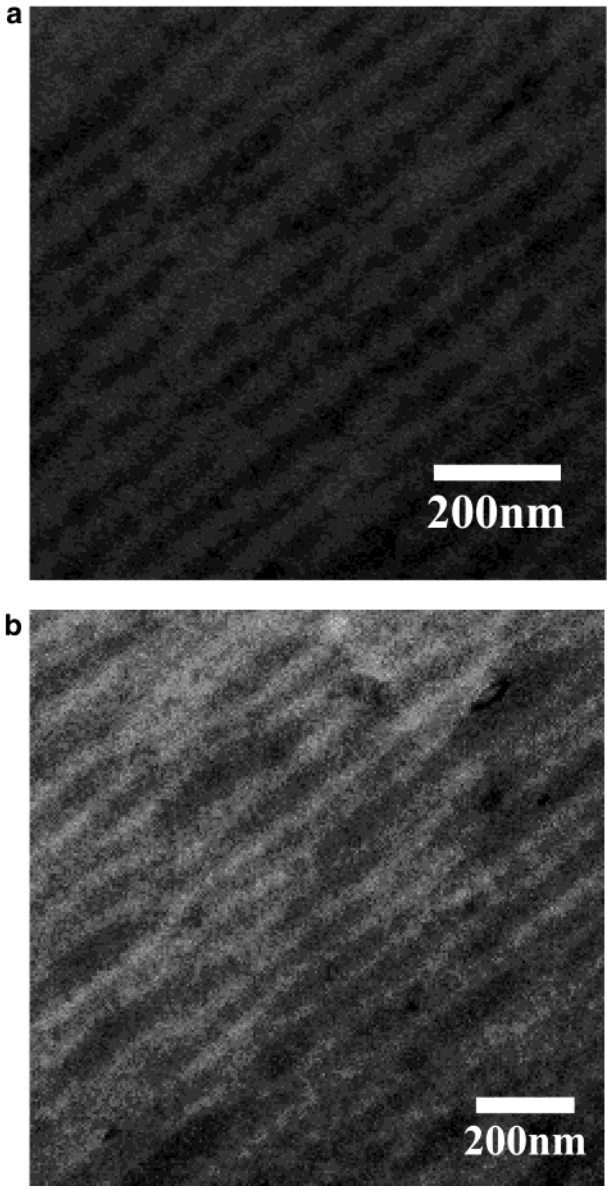

Figure 5. (a) TEM micrograph of poly[**1-*b*-(2-*b*-1**)] and (b) TEM micrograph of poly[**1-*b*-(3-*b*-1**)]. Both block copolymers have similar composition (∼50 wt % of semifluorinated block), and have similar lamellar morphologies.

Triblock copolymers with ABA architecture [50 wt % FB center block] were found to have a lamellar morphology as expected from the evaluated weight compositions reported in Table 2. The relevant TEM images are shown in Figure 5. The lamellar morphology of both samples was confirmed by SAXS which provided a pattern with a characteristic peak ratio of 1:2:3. The lamellar thickness as determined by SAXS was 70 and 75 nm in good agreement with the values obtained from TEM. The triblock copolymer poly[**1-*b*-(4-*b*-1**)] with a composition of 19 wt % fluorinated block, was found to have a disordered spherical morphology of elongated shape (with an aspect ratio of ∼2) of the fluorinated block distributed in a polystyrene matrix (see Figure 6). The ellipsoidal, rather than spherical, shape of the LC domains was attributed to the interplay between the microphase separation and liquid crystalline self-organization in the nanometer length scale.

In general, for a spherical morphology the energy of the interface between block domains drives the minor component of the block copolymer to assume a spherical

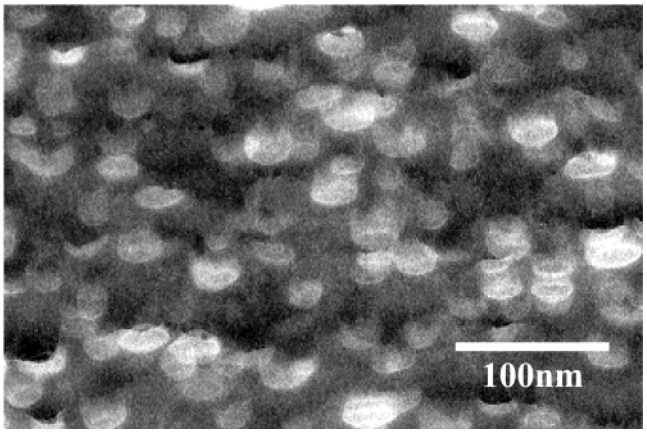

Figure 6. TEM micrograph of poly[**1-*b*-(4-*b*-1**)]. Semifluorinated block forms elongated spheres due to the LC mesophase inside the spheres.

shape in order to minimize the interfacial energy. On the other hand, for a spherical morphology formed by a liquid-crystalline smectic sub-microstructure arising from the self-assembly of mesogenic side units of the minor component of the block copolymer, the smectic mesophase must form within the limited space of the spheres; hence breaking the circular curvature may occur in order to achieve efficient packing of the mesogenic units. The tradeoff between the tendency to produce perfectly spherical microdomains and the tendency to produce a well-ordered layered array of mesogens within the spherical microdomains, may result in the occurrence of a spherical morphology characterized by elongated spherical features, as observed for poly-[**1-*b*-(4-*b*-1**)]. To support the above speculation, wide-angle X-ray (WAXD) patterns of poly[**1-*b*-(4-*b*-1**)] and corresponding diblock copolymer poly(**1-*b*-4**) and homopolymer poly(**4**), are shown in Figure 7. The WAXD pattern of poly(**1-*b*-4**), characterized by a spherical morphology with spheres of poly(styrene) placed in a fluorinated LC matrix, showed inner reflections as sharp and intense as the homopolymer, poly(**4**). On the other hand, poly[**1-*b*-(4-*b*-1**)], characterized by a spherical morphology with spheres of fluorinated LC block placed in a poly(styrene) matrix, showed more diffuse and weaker features than those of poly(**1-*b*-4**) and poly-(**4**), likely due to the packing frustrations within the LC spherical domains. We believe that this is the first time that this kind of elongated sphere morphology has been observed for coil-LC side-chain block copolymers.

Surface Orientation Studies. The surface structure of these semifluorinated polymers was characterized by near-edge X-ray absorption fine structure (NEXAFS) analysis. This technique has become a useful tool for studying molecular orientation at the surface of a variety of materials.[23] In our previous investigations, we have studied the orientational behavior of liquid crystalline poly(styrene-*b*-isoprene) block copolymers bearing semifluorinated alkyl side groups,[18,21,22] concluding that the net orientation toward the surface normal of the pendent fluorinated groups on the surface region (upper 2 nm) of a thin polymer film is controlled by the chemical architecture of the semifluorinated side chains. NEXAFS allows one to determine the order parameters S_{C-F} and S_{C-C} of the C−F and C−C bonds of the semifluorinated side groups at the surface as outlined in the appendix and the order parameter $S_{F-helix}$ of the $-CF_2-$ helix can be derived from S_{C-F} by assuming that this helix is rigid and that all the C−F bonds are oriented normal to it. The phenyl rings of the semifluorinated side chain polymers investigated here provide an additional moiety whose orientational order parameter can be investigated by NEXAFS. The details of how the various order parameters are derived are given in the Appendix.

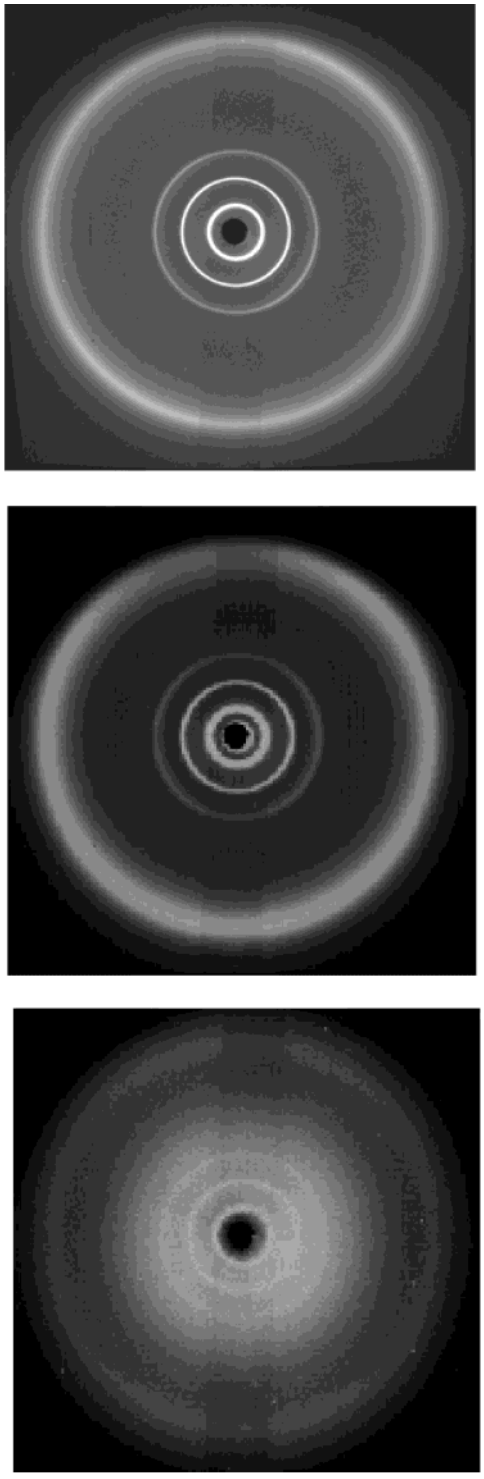

Figure 7. WAXD patterns of poly(**4**) (top), poly(**1-*b*-4**) (center), and poly[**1-*b*-(4-*b*-1**)] (bottom). The comparison of these three patterns shows that poly(**4**) and poly(**1-*b*-4**) have very strong LC mesophase while poly[**1-*b*-(4-*b*-1**)] only forms weak LC mesophase inside the elongated spherical phase shown in Figure 6.

(a) Side-Chain Modified Anionic Block Copolymers. Distinct from the previously investigated sys-

tems, the semifluorinated block copolymers of the present study contained side chains with a relatively short $-CH_2-$ spacer and an aromatic ring between the spacer and the fluorinated tail (Scheme 1.). This kind of architecture should impart to the side chains less flexibility but also an enhanced tendency to self-assemble due to the presence of the aromatic core, when compared to semifluorinated alkyl side chains. If this is indeed the case, one should see a strong correlation between the orientational order parameter S_{C-F} of the C−F bonds of the side chain and the order parameter S_{π^*} of the normal to the phenyl ring. For example if the $-(CF_2)-$ helix were collinear with the phenyl ring part of the mesogen, and both were perfectly oriented along the surface normal, S_{C-F} and S_{π^*} would both equal $-1/2$. Even if the mesogen orientation were not perfect, one would expect that the S_{CF} and S_{π^*} should be equal and negative if the helix and phenyl group were rigidly collinear. On the other hand, if the $-(CF_2)-$ helix were not collinear with the phenyl ring, S_{C-F} and S_{π^*} would be negative but different in absolute value and their comparison would show us how strongly coupled the fluorocarbon substituent and the phenyl ring are in the liquid crystalline surface layer.

As an example, typical partial electron yield (PEY) spectra for different angles θ between the polarization vector of the X-ray beam and the normal to the surface, as well as typical fluorescence yield (FY) spectra of poly(**1-*b*-6**) are shown in Figure 8a,b. The comparison of the FY spectra with the PEY spectra also demonstrates that the surface is highly enriched in C−F bonds. By analyzing both the PEY and FY spectra, characteristic resonance peaks could be clearly identified and attributed to the different chemical bonds. The peak at $E = 284.5$ eV is associated with the 1s → π^* transition of the C═C bonds in the phenyl ring of side chains. The other peaks correspond to the 1s → σ^* transitions associated with the C−H ($E = 287.9$ eV), C−F ($E = 292.0$ eV), and C−C ($E = 294.8$ eV) bonds, respectively.

To quantify the strong orientation of these samples, NEXAFS data were analyzed, as described in the appendix,[18] to determine the orientational order parameter of the C−F bonds, S_{C-F}, the uniaxial orientational order parameter $S_{F-helix}$ of the $-CF_2-$ helix as well as the average tilt angle between the helix and the surface normal, $\tau_{F-helix}$ for all samples. The orientational order parameter S_{π^*} of the normal to the phenyl ring was also calculated. The data obtained are collected in Table 4.

As can be observed from Table 4, both sample poly(**1-*b*-5**) and poly(**1-*b*-6**) showed a remarkably high $-CF_2-$ helix orientational order parameter, with $S_{F-helix}$ of poly(**1-*b*-6**) being higher than that of poly(**1-*b*-5**). These values of $S_{F-helix}$ (0. 235 and 0.335 for poly(**1-*b*-5**) and poly(**1-*b*-6**), respectively) are higher than those showed by the previously investigated block copolymers bearing semifluorinated alkyl side chains with a comparable number of CF_2 units[18] ($S_{C-F\ helix} = 0.17-0.29$). This difference in orientational behavior can be explained on the basis of the different chemical structures in the two systems. In the present system, a phenyl group was introduced into the side chain between the main chain and fluorocarbon helix tail. The intermolecular interaction between the aromatic side chains, as well as the coupling between the phenyl ring and the C−F helix played an important role in the improved surface orientational behavior of the fluorocarbon side

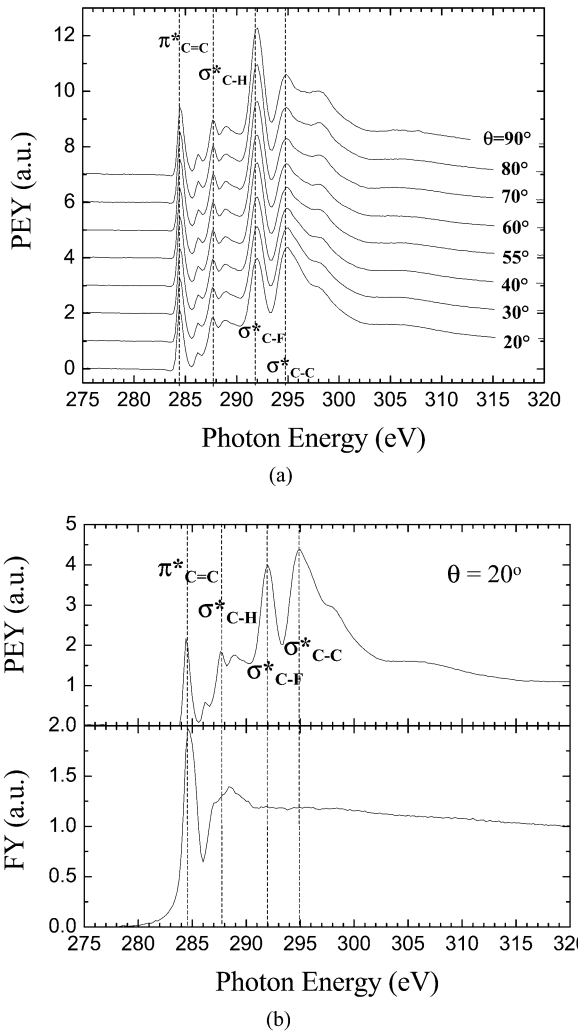

Figure 8. (a) Partial electron yield (PEY) intensity versus X-ray photon energy for angles θ between the electric field vector of the polarized X-rays and the sample normal at EGB = −150 V for sample poly(**1-*b*-6**). (b) PEY (upper part) and FY (lower part) spectra for sample poly(**1-*b*-6**) at EGB = −150 V and $\theta = 20°$. The dashed lines in the figure denote the 1s → σ^* transitions for the C−H ($E = 287.9$ eV), C−F ($E = 292.0$ eV), and C−C ($E = 294.8$ eV) bonds and the 1s → π^* transition of the C═C bond ($E = 284.5$ eV) in the phenyl ring (present in both the PEY and FY spectra).

groups of the present systems with respect to the previous ones. In fact, as can be seen in Table 4, both sample poly(**1-*b*-5**) and poly(**1-*b*-6**) showed orientation parameters S_{π^*} of the normal to the phenyl ring which were only slightly smaller than that of C−F bonds, S_{C-F}, the S_{π^*} of poly(**1-*b*-6**) being higher than that of poly(**1-*b*-5**).

The intermolecular interaction of the phenyl rings also increased the stability of the LC mesophase. In situ WAXD at elevated temperatures was carried out to determine the mesophase transition temperatures which are listed in Table 3. As can be seen from Table 3, the LC phases of the polymers with semifluorinated side chains containing phenyl group have high isotropic transition temperatures. In fact, typical isotropic transition temperatures for the semifluorinated alkyl block copolymers were about 70 °C,[1] whereas the isotropic transition temperatures for poly(**1-*b*-5**) and poly(**1-*b*-6**) were about 210 °C. Furthermore, the improved self-assembly behavior of the present system is also reflected in the high stability of the surface toward reconstruction

Table 4. Surface Orientational Order Parameters of Side Chain Modified Block Copolymers via Anionic Polymerization

sample	S_{π^*}	S_{C-F}	$S_{F-helix}$	$\langle\tau_{F-helix}\rangle$ (deg)
poly(**1-*b*-5**)	-0.101 ± 0.009	-0.117 ± 0.011	0.234 ± 0.022	45.6 ± 0.8
poly(**1-*b*-6**)	-0.112 ± 0.012	-0.168 ± 0.015	0.336 ± 0.030	41.7 ± 1.1

Table 5. Surface Orientational Order Parameters of Block Copolymers and Corresponding Homopolymers via Controlled Radical Polymerization

sample	S_{π^*}	S_{C-F}	$S_{F-helix}$	$\langle\tau_{F-helix}\rangle$ (deg)
poly(**2**)	-0.099 ± 0.011	-0.034 ± 0.013	0.068 ± 0.026	52.0 ± 1.0
poly(**3**)	-0.120 ± 0.008	-0.066 ± 0.016	0.132 ± 0.032	49.6 ± 1.3
poly(**4**)	-0.174 ± 0.011	-0.174 ± 0.015	0.348 ± 0.030	41.3 ± 1.2
poly(**1-*b*-2**)	-0.075 ± 0.014	-0.030 ± 0.016	0.060 ± 0.032	52.4 ± 1.3
poly(**1-*b*-3**)	-0.127 ± 0.008	-0.069 ± 0.014	0.138 ± 0.028	49.3 ± 1.1
poly(**1-*b*-4**)	-0.187 ± 0.017	-0.176 ± 0.007	0.352 ± 0.014	41.1 ± 0.5
poly[**1-*b*-(2-*b*-1**)]	-0.081 ± 0.010	-0.023 ± 0.011	0.046 ± 0.022	52.9 ± 0.9
poly[**1-*b*-(3-*b*-1**)]	-0.128 ± 0.012	-0.102 ± 0.014	0.204 ± 0.028	46.8 ± 1.1
poly[**1-*b*-(4-*b*-1**)]	-0.168 ± 0.009	-0.151 ± 0.009	0.302 ± 0.018	43.0 ± 0.7

Table 6. Surface Orientational Order Parameters of Block Copolymers before and after Exposure to Water

	before H_2O exposure		after H_2O exposure	
sample	$S_{F-helix}$	$\langle\tau_{F-helix}\rangle$ (deg)	$S_{F-helix}$	$\langle\tau_{F-helix}\rangle$ (deg)
poly(**1-*b*-5**)	0.234 ± 0.022	45.6 ± 0.8	0.163 ± 0.029	48.4 ± 1.2
poly(**1-*b*-6**)	0.336 ± 0.030	41.7 ± 1.1	0.207 ± 0.025	46.7 ± 1.0
poly(**4**)	0.348 ± 0.030	41.3 ± 1.2	0.344 ± 0.033	41.4 ± 1.3
poly(**1-*b*-4**)	0.352 ± 0.014	41.1 ± 0.5	0.347 ± 0.021	41.3 ± 0.8
poly[**1-*b*-(4-*b*-1**)]	0.302 ± 0.018	43.0 ± 0.7	0.307 ± 0.025	42.8 ± 0.9

upon prolonged exposure to water. Films of poly(**1-*b*-5**) and poly(**1-*b*-6**) showed rather high advancing water contact angles of about 120° and 130°, respectively. These were about 6−10° greater than the receding contact angles. The advancing contact angles were quite constant over a period of exposure to water of 25 days, as described in ref 20. The helix surface order parameter was determined by NEXAFS after a 25 day period of exposure to water and the results obtained are collected in Table 6. While the helix surface order parameter decreases to a certain extent after water exposure, it still remains remarkably high. This finding indicates a relatively small loss of orientation of the fluorinated side chains. The critical surface tensions as determined by the Zisman method turned out to be low, e.g., 10 dyn/cm and 8.7 dyn/cm for poly(**1-*b*-5**) and poly(**1-*b*-6**), respectively. Figure 9 shows the Zisman plot of the block copolymers in contact with a series of standard hydrocarbon liquids. All the above evidence pointed to the presence of remarkably stable, low energy fluorinated surfaces.

(b) Controlled Radical Polymerization Block Copolymers. The CRP block copolymers of this study also contained side chains with an aromatic core bearing a fluorinated alkyl tail. Figure 10 shows the PEY spectra of the poly(**1-*b*-4**) diblock copolymer for different angles θ between the polarization vector of the X-ray beam and the normal to the surface. This set of PEY spectra is typical for all the CRP block copolymers, with only the magnitude of the variation in the spectra with θ changing between samples.

From a comparison between the PEY and the FY spectra, characteristic resonance peaks could be clearly identified and attributed to the different chemical bonds. In particular, the spectra showed a relatively strong peak at 284.6 eV which was attributed to the 1s$-\pi^*$ transition of the C═C bonds in the phenyl ring of the side chain.

Clearly the fact that the σ^*_{C-F} signal is maximized in passing from $\theta = 20°$ to $\theta = 90°$, while the σ^*_{C-C} decreases with increasing angle, indicates that the net orientation of the fluorocarbon segments of the side-chains is toward the surface normal, thus forming a CF_3

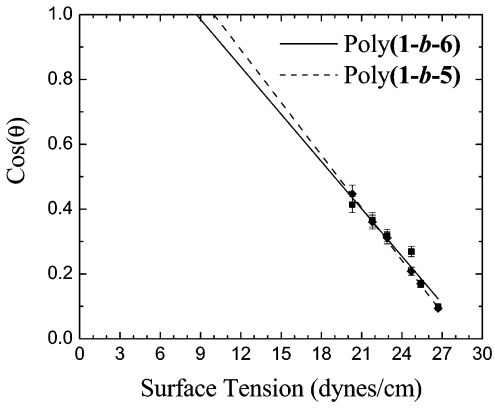

Figure 9. Zisman plot for side-chain modified block copolymers poly(**1-*b*-5**) and poly(**1-*b*-6**) constructed from contact angle measurements using a homologous series of *n*-alkanes and methyl-terminated poly(dimethylsiloxanes).

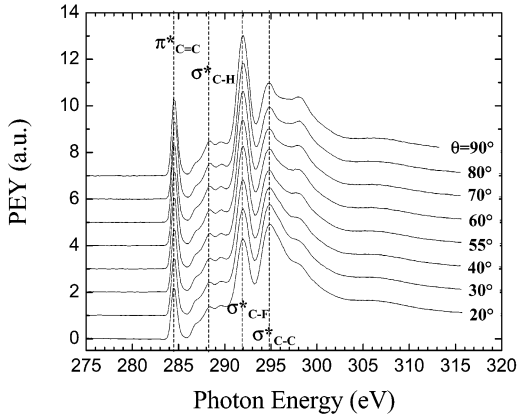

Figure 10. PEY spectra of sample poly(**1-*b*-4**) at EGB = −150 V and various sample orientations with respect to the X-ray beam, θ. The dashed lines in the figure denote the 1s → σ^* transitions for the C−H (E = 287.9 eV), C−F (E = 292.0 eV), and C−C (E = 294.8 eV) bonds and the 1s →π^* transition of the C═C bond (E = 284.5 eV) in the phenyl ring.

surface. This is indeed a general trend for all CRP block copolymers investigated. To quantify these statements, the orientational order parameters S_{C-F} and S_{π^*} of the C−F bonds and the phenyl ring normal respectively were determined. From these the uniaxial orientational order parameter $S_{F-helix}$ of the CF_2 helix as well as the average tilt angle between the helix and the surface normal, $\tau_{F-helix}$, were evaluated as described in the appendix.[18]

The calculated order parameters for the diblock copolymers poly(**1-*b*-*x***) (x = 2, 3, 4) and the triblock copolymers poly[**1-*b*-(*x*-*b*-1**)] (x = 2, 3, or 4), as well as for the corresponding reference homopolymers poly(***x***) (x = 2, 3, or 4), are collected in Table 5.

It must be pointed out that all the samples bearing a $(CF_2)_8$ tail in the side-chains, such as poly(**4**), poly(**1-*b*-4**), and poly[**1-*b*-(4-*b*-1**)], showed a remarkably high helix orientational parameter of about 0.3−0.35 with average tilt angles of about 41°, 42°, and 43°, respectively, regardless of the wt % of the fluorinated block in the copolymer. On the other hand, polymers bearing either a $(CF_2)_4$ or a $(CF_2)_6$ tail in the side-chains show much smaller helix orientational order parameters.

The above evidence is consistent with a tendency of the shorter fluorocarbon segments (n_{CF_2} = 4 or 6) to form a less well-ordered surface and bulk mesophase than the longer fluorinated alkyl groups (n_{CF_2} = 8).[20] Also, $S_{F-helix}$ (0.348, 0.352, 0.302 for poly(**4**), poly(**1-*b*-4**), and poly[**1-*b*-(4-*b*-1**)]) turned out to be higher than the previously investigated semifluorinated block copolymers[18] ($S_{F-helix}$ = 0.176−0.286).

The orientational order parameters S_{π^*} of the normal to the phenyl rings were also studied and the data are listed in Table 5. The S_{π^*} of the phenyl ring normal turned out to be higher than (n_{CF_2} = 4 or 6), or approximately equal to (n_{CF_2} = 8) the orientation order parameter S_{C-F} of C−F bonds. The values of S_{π^*} showed the same trend as that of $-CF_2-$ helix, i.e., the longer the fluorocarbon group the higher S_{π^*} regardless of the wt % of the fluorinated block.

The present system shows dramatically improved surface orientation parameters, as compared to those of the previous side-chain semifluorinated block copolymers. Similar to the aromatic side chain modified block copolymers discussed in the previous section, the improvement resulted from the intermolecular interaction of the phenyl rings and the coupling between the phenyl group and the fluorocarbon helix tail.

In particular, when the number of CF_2 units was equal to eight, the S_{π^*} was almost equal to S_{C-F} (as shown in Figure 11), strongly suggesting that the phenyl ring and the $-CF_2-$ helix were almost collinear. This strong coupling of phenyl group with the C−F helix made both S_{C-F} and S_{π^*} significantly higher than the orientation parameters of other samples. The introduction of a phenyl group in the side chain also dramatically increased the thermal stability of the LC mesophase. As shown in Table 3, the CRP block copolymers typically have an isotropic transition temperature well above 130°C, whereas the previously studied semifluorinated alkyl side chain block copolymers typically have an isotropic transition temperature of 70 °C.

Furthermore, the improved surface self-assembly behavior of the fluorinated aromatic side chains is correlated with a high stability of the surface toward reconstruction upon prolonged exposure to water. Films of poly(1-*b*-2), poly(**1-*b*-3**) and poly(**1-*b*-4**) showed values

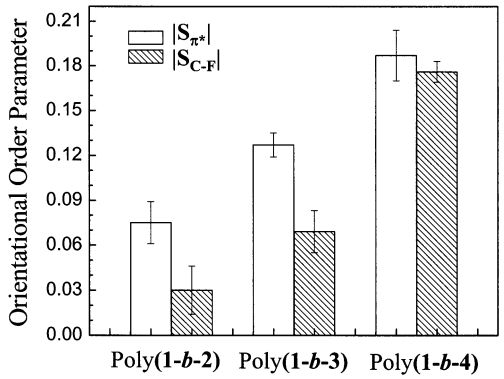

Figure 11. Direct comparison of orientational order parameters (S_{π^*} and S_{C-F}) for block copolymers poly(**1-*b*-2**), poly(**1-*b*-3**) and poly(**1-*b*-4**) produced by controlled radical polymerization. The y-coordinate is plotted as the absolute value of the (negative) orientational order parameters. When the number of $-CF_2-$ units is equal to 8, S_{π^*} is almost equal to S_{C-F} and the phenyl ring is collinear with the CF_2 helix. The homopolymer poly(**4**), triblock copolymer poly[**1-*b*-(4-*b*-1**)] and anionically polymerized block copolymer poly(**1-*b*-6**) also have eight $-CF_2-$ units and showed the same strong coupling behavior between the phenyl ring and $-CF_2-$ helix.

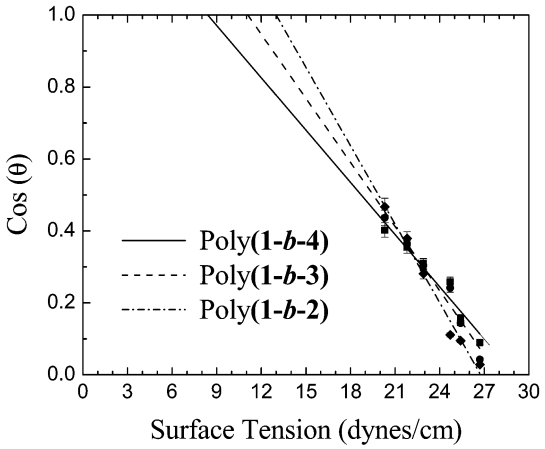

Figure 12. Zisman plot for block copolymers poly(**1-*b*-2**), poly(**1-*b*-3**), and poly(**1-*b*-4**) produced by controlled radical polymerization.

of the advancing contact angle in the range 94°−111° that depended on the length of the fluorinated side-group. In all cases the receding contact angles were lower by 5−6°, which pointed to formation of quite stable fluorinated surfaces.

Poly(**4**) and the corresponding diblock and triblock copolymers, were characterized by NEXAFS after 25 days of water exposure to check for possible variation of the order parameter of the surface upon contact with water. The calculated helix order parameters, $S_{F-helix}$, are collected in Table 6. Remarkably, $S_{F-helix}$ remained high and unchanged after exposure to water both for the homopolymer and corresponding di- and triblock copolymers.

The critical surface tensions were determined by the Zisman method, and are 13, 11.2, and 8.4 dyn/cm for poly(**1-*b*-2**), poly(**1-*b*-3**), and poly(**1-*b*-4**), respectively. Figure 12 shows the Zisman plot of the block copolymers in contact with a series of standard hydrocarbon liquids. The values of critical surface tension turned out to be about the same for the homopolymers, the block copolymers and the triblock copolymers.

Figure 13 shows a comparison of the critical surface tensions for all the diblock copolymers plotted against

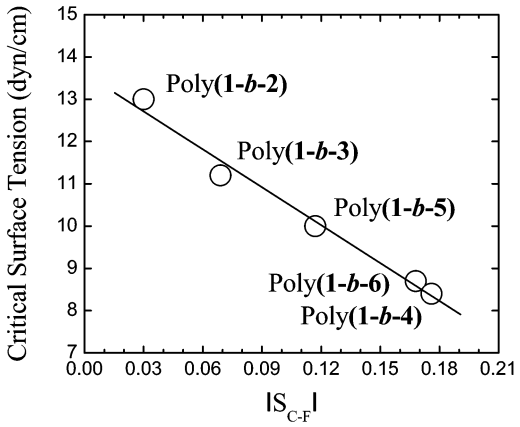

Figure 13. Critical surface tensions from Zisman plots (Figures 9 and 12) versus the absolute value of the (negative) orientational order parameters (S_{C-F}) for the diblock copolymers. These results show that surfaces with more highly ordered $-CF_2-$ helices have lower surface energies.

the absolute value of the (negative) orientational order parameter S_{C-F}. These results show that there is a very strong correlation between the order of $-CF_2-$ helix and the critical surface tension of the fluorinated surface. The more highly aligned the C−F bonds are with the plane of the surface (the more aligned the helix axis is with the surface normal), the lower the critical surface tension of that surface is. If the orientational order is high, the surface will be mainly populated with $-CF_3$ groups and thus it will have the minimum surface energy.

All the above evidence also shows that the samples containing a fluorinated tail with eight $-CF_2-$ units allow the creation of remarkably stable ultralow energy surfaces, regardless of the fluorinated block composition. This makes these materials excellent candidates for blending applications in which a minimum fluorine content can be used to create materials with very stable low energy surfaces.

Conclusions

In summary, two classes of new narrow polydispersity poly(styrene)-based block copolymers bearing fluorinated aromatic side chains were produced to have ultra stable low energy surfaces. The effects of the phenyl ring and the fluorocarbon pendent groups on the surface and bulk structure of materials were investigated. NEXAFS measurements showed high $-CF_2-$ helix surface orientation parameters which remained relatively unchanged after prolonged exposure of the polymer films to water. The surface orientational order parameters of the aromatic fluorinated side-chain block copolymers also proved to be consistently higher than the previously investigated semifluoroalkyl side-chain block copolymers.

NEXAFS also allowed us to determine the surface orientational order parameter S_{π^*} of the phenyl group normal. In both types of polymers, the CF_2 helix surface orientational order parameter turned out to be strongly coupled to the phenyl ring order parameter when the number of CF_2 groups was equal to eight.

In particular, in the anionically polymerized block copolymers S_{π^*} turned out to be slightly smaller than the S_{C-F}, whereas in the CRP block copolymers S_{π^*} was slightly larger than S_{C-F}. This difference can be explained on the basis of the different chemical structures. In particular, the flexible spacer between the phenyl ring and the polymer main chain in the former system could give the phenyl ring more flexibility, thus resulting in a smaller S_{π^*} value. On the other hand, the phenyl ring directly linked to the polymer backbone in the latter system, would result in a less flexible side chain thus leading to a larger S_{π^*} value.

Clearly the introduction of an aromatic ring between the polymer backbone and the fluorocarbon pendent group turned out to improve the self-assembly behavior of the fluorinated part of the side chain at the surface. This self-assembly produces highly hydrophobic $-CF_3$ surfaces that are remarkably stable toward reconstruction upon exposure to water.

Acknowledgment. The authors thank the Italian Ministry of University and Scientific Research (PRIN 2001034479) and the Office of Naval Research Grant No. N00014-92-J-1246, and the National Science Foundation, Division of Materials Research, Polymers Program (Grants DMR-9803738 and DMR-9972863) for partial support of this work. The Cornell Center for Materials Research and the Materials Research Laboratory of UCSB (both funded by the NSF-DMR-MRSEC Program), the Cornell High Energy Synchrotron Source (CHESS) and the National Synchrotron Light Source, Brookhaven National Laboratory, which is supported by the U.S. Department of Energy, Division of Materials Sciences and Division of Chemical Sciences, are also gratefully acknowledged for the use of the facilities.

Appendix: Order Parameters from NEXAFS Data

To analyze the NEXAFS spectra in detail we fit these spectra to a series of Gaussian curves representing the 1s → π^* and the various 1s → σ^* transitions and a step function rising at the excitation edge for carbon as prescribed by Outka et al.[24] The magnitudes of these Gaussians give the PEY intensities $I(\theta)$ of the 1s → π^* and the various 1s → σ^* transitions. We define separate molecular orientation factors f_x, f_y, and f_z for the phenyl ring normal, the C−F bond direction and the C−C bond direction, as suggested by Stöhr and Samant.[25] These molecular orientation factors are given by

$$f_z = \int \{\cos^2 \alpha[f(\alpha)]\}\, d\Omega$$

and

$$f_x = f_y = \frac{1 - f_z}{2}$$

where z is an axis normal to the film surface and x and y are orthogonal axes in the plane of the surface while α is the angle between the z direction and the relevant molecular axis (π^* orbital direction = phenyl ring normal or σ^* orbital direction = C−F or C−C bond direction). The molecular axis distribution function $f(\alpha)$ is normalized so that $\int f(\alpha)\, d\Omega = 1$ and thus $f_x + f_y + f_z = 1$. A uniaxial order parameter S can then be defined as

$$S = \frac{1}{2}(3f_z - 1)$$

where S ranges from 1 (π^* or σ^* orbital direction perfectly aligned with z) to $-1/2$ (π^* or σ^* orbital direction in the plane of the surface). This treatment

assumes that there is rotational isotropy about *z*, i.e., that direction has fiber symmetry, a good assumption for our films which should have no preferred direction in the film plane. For such symmetry the PEY intensity must have the following form:

$$I(\theta) = A + B \sin^2 \theta \quad (1)$$

and the orientational order parameter is given by

$$S = -\frac{P^{-1}B}{3A + (3 - P^{-1})B} \quad (2)$$

where P is the polarization factor of the soft X-ray beam (=0.85 in our case). We have extracted A and B values by fitting the π^*, σ^*_{C-F}, and σ^*_{C-C} data to eq 1 and have then used eq 2 to extract the order parameters S_{π^*}, S_{CF}, and S_{CC} of the phenyl ring normal, the C−F bond axis and the C−C bond axis, respectively. If we assume that the $-CF_2-$ bonds form a helix with the C−F bonds normal to the helix axis it is easy to show that the orientational order parameter of the helix $S_{F-helix}$ is given by[26]

$$S_{F-helix} = -2S_{CF}$$

Finally, the average angle $\langle\tau_{F-helix}\rangle$ the axis of the helix makes to the surface normal is given by[26]

$$\langle\tau_{F-helix}\rangle = \sin^{-1}\{[(4S_{CF} + 2)/3]^{1/2}\}$$

References and Notes

(1) Wang, J.; Mao, G.; Ober, C. K.; Kramer, E. J. *Macromolecules* **1997**, *30*, 1906.
(2) Yamabe, M.; *Makromol. Chem., Macromol. Symp.* **1992**, *64*, 11.
(3) Koemehl, G.; Fluthwedel, A.; Schafer, H.; *Makromol. Chem.* **1992**, *193*, 157.
(4) Brady, R. F.; *Prog. Org. Coat.* **1999**, *35*, 31.
(5) Auman, B. C.; Higley, D. P.; Schere, K. V.; McCord, E. F.; Shaw, W. H. *Polymer* **1995**, 36, 651.
(6) McCulloch, I.; Yoon, H. *J. Polym. Sci., Part A: Polym. Chem.* **1995**, *33*, 1177.
(7) Gaynor, J.; Scheueneman, G.; Murata, N. *J. Polym. Sci.* **1993**, *31*, 1645.
(8) Maruno, T.; Nakamura, K.; Murata, N. *Macromolecules* **1996**, *29*, 2006.
(9) Ajroldi, G. *Chim. Ind.* (*Milan*) **1997**, *79*, 484.
(10) Brady, R. F., Jr; Griffith, J. R.; Love, K. S.; Field, D. E. *J. Coat. Technol.* **1987**, *59*, 755.
(11) Brady, R. F., Jr. *J. Coat. Technol.* **2000**, *72*, 45.
(12) Passaglia, E.; Aglietto, M.; Ciardelli, F.; Mendez, B. *Polym. J.* **1994**, *26*, 1118.
(13) Hopken, J.; Moller, M. *Macromolecules* **1992**, *25*, 1461.
(14) Wilson, L. M.; Griffin, A. C. *Macromolecules* **1994**, *27*, 1928.
(15) Honeychuck, R. V.; Ho, T.; Wynne, K. J.; Nissan, R. A. *Chem. Mater.* **1993**, *5*, 1299.
(16) Boutevin, B.; Caporiccio, G.; Guida-Pietrasanta, F.; Ratsimihety, A. *Macromol. Chem. Phys.* **1998**, *199*, 61.
(17) Mao, G.; Wang, J.; Clingman, S. R.; Ober, C. K.; Chen, J. T.; Thomas, E. L. *Macromolecules* **1997**, *30*, 2556.
(18) Xiang, M.; Li, X.; Ober, C. K.; Char, K.; Genzer, J.; Sivaniah, E.; Kramer, E. J.; Fisher, D. A. *Macromolecules* **2000**, *33*, 6106.
(19) Dhamodaran, R.; Iyengar, R.; Perutz, S. M.; Dai, C. A.; Ober, C. K.; Kramer, E. J. *Macromolecules* **1996**, *29*, 1229.
(20) Andruzzi. L.; Chiellini, E.; Galli, G.; Li, X.; Kang, S. H.; Ober, C. K. *J. Mater. Chem.* **2002**, *12*, 1684.
(21) Genzer, J.; Sivaniah, E.; Kramer, E. J.; Wang, J.; Korner, H.; Xiang, M.; Char, K.; Ober, C. K.; DeKoven B. M.; Bubeck, R. A.; Chaudhury, M. K.; Sambasivan, S.; Fisher, D. A. *Macromolecules* **2000**, *33*, 1882.
(22) Genzer, J.; Sivaniah, E.; Kramer, E. J.; Wang, J.; Korner, H.; Char, K.; Ober, C. K.; DeKoven, B. M.; Bubeck, R. A.; Fisher, D. A.; Sambasivan, S. *Langmuir* **2000**, *16*, 1993.
(23) Butoi, C. I.; Mackie, N. M.; Barnd, J. L.; Fisher, E. R.; Gamble, L. J.; Castner, D. G. *Chem. Mater.* **1999**, *11*, 862−864. Castner, D. G.; Lewis, K. B., Jr.; Fischer, D. A.; Ratner, B. D.; Gland, J. L. *Langmuir* **1993**, *9*, 537. Stöhr, J. *NEXAFS Spectroscopy*; Springer-Verlag: Berlin, 1992.
(24) Outka, D.; Stöhr, J.; Rabe, J.; Swalen, J. D. *J. Chem. Phys.* **1988**, *88*, 4076.
(25) Stöhr, J.; Samant, M. G.; *J. Electron Spectrosc. Relat. Phenom.* **1999**, *98*−*99*, 189.
(26) Hayakawa, T.; Wang, J.; Xiang, M.; Li, X.; Ueda, M.; Ober, C. K.; Genzer, J.; Sivaniah, E.; Kramer, E. J.; Fischer, D. A. *Macromolecules* **2000**, *33*, 8012.

MA020463K